Two-fluid tokamak equilibria with reversed magnetic shear and sheared flow [1]

G. Poulipoulis[†2], G. N. Throumoulopoulos[†3], H. Tasso[⋆4]

[†] *University of Ioannina, Association Euratom - Hellenic Republic, Section of Theoretical Physics, GR 451 10 Ioannina, Greece*

[⋆] *Max-Planck-Institut für Plasmaphysik, Euratom Association, D-85748 Garching, Germany*

Abstract

The aim of the present work is to investigate tokamak equilibria with reversed magnetic shear and sheared flow, which may play a role in the formation of internal transport barriers (ITBs), within the framework of two-fluid model in cylindrical geometry. The study is based on exact self-consistent solutions in cylindrical geometry by means of which the impact of the magnetic shear, s, and the "toroidal" (axial) and "poloidal" (azimuthal) ion velocity components, v_{iz} and $v_{i\theta}$, on the radial electric field, E_r, its shear, $|dE_r/dr|$, and the shear of the $\mathbf{E}\times\mathbf{B}$ velocity, $\omega_{\mathbf{E}\times\mathbf{B}} \equiv |d/dr(\mathbf{E}\times\mathbf{B}/B^2)|$, is examined. For a wide parametric regime of experimental concern it turns out that the contributions of the v_{iz}, $v_{i\theta}$ and pressure gradient (∇P_i) terms to E_r, $|E_r'|$ and $\omega_{\mathbf{E}\times\mathbf{B}}$ are of the same order of magnitude. The contribution of the ∇P_i term is missing in the framework of magnetohydrodynamics (MHD) [G. Poulipoulis et al. Plasma Phys. Control. Fusion **46** (2004) 639]. The impact of s on $\omega_{\mathbf{E}\times\mathbf{B}}$ through the ∇P_i term is stronger than that through the velocity terms; in particular for constant B_z the ion pressure gradient contribution to $\omega_{\mathbf{E}\times\mathbf{B}}$ at the point where $dE_r/dr = 0$ scales as $(1-s)(2-s)$, whereas the ion flow contributions to $\omega_{\mathbf{E}\times\mathbf{B}}$ scales as $(1-s)$. The results indicate that, alike MHD, the magnetic shear and the sheared toroidal and poloidal velocities act synergetically in producing electric fields and therefore $\omega_{\mathbf{E}\times\mathbf{B}}$ profiles compatible with ones observed in discharges with ITBs; owing to the ∇P_i term, however, the impact of s on E_r, $|E_r'|$ and $\omega_{\mathbf{E}\times\mathbf{B}}$ is stronger than that in MHD.

[1] A preliminary version of this study was presented in the 10th European Fusion Theory Conference (Helsinki, Finland, 8-10 September 2003).

[2] me00584@cc.uoi.gr

[3] gthroum@cc.uoi.gr

[4] het@ipp.mpg.de

Introduction

Tokamak discharges with improved energy and particle confinement properties in connection with internal transport barriers (ITBs) have certain attractive features, such as a large bootstrap current fraction, which suggest a potential route to steady-state mode of operation desirable for fusion power plants. Long quasi-steady or steady ITB states have been obtained in different tokamaks, e.g ASDEX Upgrade [1, 2], JT-60U [3], Tore-Supra [4], and JET [5] where ITBs were maintained for up to 11 s. The ITBs usually are associated with reversed magnetic shear profiles [6],[7] and their main characteristics are steep pressure profiles in the barrier region [8] and radial electric fields associated with sheared flows [9, 10]. The mechanism responsible for the formation of ITBs and the underlying physics is not completely understood. Most theoretical models supported by experimental observations rely on suppression of microinstability induced transport in connection with reversed magnetic shear, $s < 0$, sheared flow, radial electric field, E_r, its shear, $|E_r'|$, and most importantly the $\mathbf{E} \times \mathbf{B}$ velocity shear,

$$\omega_{\mathbf{E}\times\mathbf{B}} = \left| \frac{d}{dr} \frac{\mathbf{E} \times \mathbf{B}}{B^2} \right|. \tag{1}$$

In particular the $\mathbf{E}\times\mathbf{B}$ velocity shear may lead to a reduction in the amplitude of turbulent fluctuations, even to their suppression, or to a decrease in the radial correlation lengths [11]. An expression for $\omega_{\mathbf{E}\times\mathbf{B}}$ related to a criterion for the stabilization of microturbulence in a tokamak has been derived in Ref. [12]. Another criterion for turbulence suppression in terms of $\omega_{\mathbf{E}\times\mathbf{B}}$ was reported in Ref. [13]. Also, contributions of the toroidal velocity and the density and temperature gradients to $\omega_{\mathbf{E}\times\mathbf{B}}$ in ITB discharges of JET have been obtained in Ref. [14]. Although there are experimental observations supporting this scenario, the overall experimental evidence up to date is rather complicated, not universal in the various tokamak machines and has not made clear whether the reversed magnetic shear or the sheared flow (toroidal or poloidal) are more important for the ITB formation. According to recent measurements of the poloidal rotation velocity across ITBs in JET this velocity is an order of magnitude higher than neoclassical predictions for the thermal particles in the ITB region and has large impact on the measured radial electric field profile [15]. Discrepancy of the measured poloidal velocities from neoclassical predictions before, during and after the transport bifurcation associated with enhanced reversed shear plasmas was reported in Refs.[16, 17]. Further discussion on these issues is made in the Introduction of Ref. [18]. Also, the experimental and theoretical knowledge on discharges with ITBs was reviewed recently in Refs. [11] and [19].

In a previous work [18] we studied tokamak magnetohydrodynamic (MHD) equilibrium states with reversed magnetic shear and sheared flow in cylindrical geometry. In particular, presuming that E_r, E_r' and $\omega_{\mathbf{E}\times\mathbf{B}}$ are of relevance to the formation of ITBs we examined how these quantities are affected by the magnetic shear and sheared flow and found that the latter quantities act synergetically in increasing $\omega_{\mathbf{E}\times\mathbf{B}}$ with the impact of the flow, in particular the poloidal one, being stronger than that of the magnetic shear, s. In view of complicated experimental evidence and incomplete theoretical understanding, the present work aims in a first step at extending our previous MHD study [18] to the framework of the two fluid model. This model is advantageous over MHD in that the contribution of the ion pressure gradient (∇P_i) term to E_r, contribution which is missing in MHD, can be obtained from the ion (or electron) momentum equation. In addition the

current density can be expressed self-consistently in terms of the ion and electron fluid velocities. Also, we shall examine the impact of certain local characteristics of the safety factor profile, i.e. the minimum of q and its position, on the aforementioned quantities (not addressed in Ref. [18]) and the relative sign of the "toroidal" (axial) ion velocity, v_{iz}, "poloidal" (azimuthal) ion velocity, $v_{i\theta}$, and toroidal magnetic field, B_z. It turns out that, owing to the ∇P_i term, the impact of s on E_r, E_r' and $\omega_{\mathbf{E}\times\mathbf{B}}$ is stronger than that in MHD. The contribution of both flow components, however, remains significant. In addition in many cases s enhances the velocity contribution to these quantities which, alike in MHD, indicates a synergism of s and the flow.

The work will be conducted through the following steps. Exact solutions of a slightly reduced set of two-fluid equilibrium equations for a cylindrical magnetically confined plasma are constructed in section 2 by prescribing the profiles of certain free quantities, including the safety factor and the toroidal and poloidal ion velocities, in accord with ITB experimental ones. Then in section 3 we examine the impact of s, the velocity, the velocity shear, the local characteristics of q, and the relative signs of the velocity components and B_z on E_r, E_r' and $\omega_{\mathbf{E}\times\mathbf{B}}$. The characteristics of the pressure and toroidal current density are also briefly discussed. The conclusions are summarized in section 4.

2. Two-fluid cylindrical equilibria with reversed magnetic shear

The two-fluid equilibrium states of an ideal quasineutral plasma are governed by the following set of equations written in Gaussian units with both 4π and the velocity of light being set to unity:

$$\nabla \cdot (n\mathbf{v}_\alpha) = 0, \tag{2}$$

$$m_\alpha n_\alpha (\mathbf{v}_\alpha \cdot \nabla)\mathbf{v}_\alpha = -\nabla P_\alpha + q_\alpha n_\alpha (\mathbf{E} + \mathbf{v}_\alpha \times \mathbf{B}), \tag{3}$$

$$\mathbf{v}_\alpha \cdot \nabla T_\alpha = 0, \tag{4}$$

$$Z_i n_i \approx n_e = n, \tag{5}$$

$$\nabla \times \mathbf{E} = 0, \tag{6}$$

$$\nabla \cdot \mathbf{B} = 0, \tag{7}$$

$$\nabla \times \mathbf{B} = \sum_\alpha n_\alpha q_\alpha \mathbf{v}_\alpha = \mathbf{J}, \tag{8}$$

where the index α denotes the particle species ($\alpha = i$ for ions and e for electrons); n is the plasma density in connection with the quasi-neutrality condition (5); q_α is the charge of each particle species with Z_i being the atomic number. The rest of the notation is standard. The energy equation (4), associated with the fact that for fusion plasmas the heat conduction along $\mathbf{B}$ is large and therefore the temperature becomes uniform on magnetic surfaces on a fast time scale, is particularly appropriate for electrons. For ions one alternatively can use an adiabatic energy equation:

$$\mathbf{v}_i \cdot \nabla P_i + \gamma P_i \nabla \cdot \mathbf{v}_i = 0. \tag{9}$$

Compared with the respective set of MHD equations (see for example Eqs. (2)-(6) of Ref. [18]) Eqs. (2-8) are advantageous in two respects: (i) the momentum equation includes the electric field and therefore the pressure gradient contribution to $\mathbf{E}$ can be calculated from

this equation; this contribution is missing in the frame of MHD because $\mathbf{E}$ is calculated by Ohm's law, $\mathbf{E} + \mathbf{v} \times \mathbf{B} = 0$, and (ii) the current density $\mathbf{J}$ is related self-consistently to the fluid species velocities [Eq. (8)].

The system under consideration is a cylindrical plasma of circular cross-section confined by a magnetic field having toroidal and poloidal components B_z and B_θ respectively. Also the velocity has toroidal and poloidal components and the electric field is radial. Because of symmetry any equilibrium quantity depends solely on the radial distance r; therefore Eqs. (2), (4)[and (9)], (6), and (7) are identically satisfied. Also the flow for both fluid species is incompressible ($\nabla \cdot \mathbf{v}_\alpha = 0$). Under these considerations 6 out of the 12 scalar quantities remain free and can be prescribed.

Adding Eq. (3) for ions and electrons yields the MHD momentum equation

$$\frac{d}{dr}\left(P + \frac{B_\theta^2 + B_z^2}{2}\right) + \left(1 - M_\theta^2\right)\frac{B_\theta^2}{r} = 0, \tag{10}$$

where

$$M_\theta \equiv \left[\frac{n_i m_i v_{i\theta}^2 + n_e m_e v_{e\theta}^2}{B_\theta^2}\right]^{1/2}$$

is the poloidal Mach number. Because of symmetry the toroidal velocity as well as the velocity shear (of both toroidal and poloidal components) do not appear in (10). It is convenient to use (10) instead of (3) for the electrons. Therefore the slightly reduced set of equilibrium equations we will use in the following consists of Eqs. (2), (3), (4) for ions only, (5), (6), (7), (8), and (10). By expressing B_θ in terms of the safety factor, $q = rB_\theta/(R_0 B_z)$, with $2\pi R_0$ associated with the length of the plasma column, and introducing the normalized radius $\rho = r/r_0$ with r_0 corresponding to the plasma surface, Eq. (10) can be put in the form

$$P'(\rho) = -B_z(\rho)B_z'(\rho)\left[1 + \left(\epsilon\frac{\rho}{q(\rho)}\right)^2\right] + \left[M_\theta(\rho)^2 + s(\rho) - 2\right]\frac{\rho}{r_0}\left(\epsilon\frac{B_z(\rho)}{q(\rho)}\right)^2. \tag{11}$$

Here, $\epsilon = r_0/R_0$ is the inverse aspect ratio and $s(\rho) = (r/q)(dq/dr)$ the magnetic shear.

On account of typical experimental ITB profiles we prescribe the quantities q, B_z, $v_{i\theta}$, v_{iz} and n as follows:
Reversed magnetic shear profile:

$$q(\rho) = q_c\Big(1 - \frac{3\Delta q}{q_c}\frac{r_0^2}{r_{min}^2}\rho^2 + \frac{2\Delta q}{q_c}\frac{r_0^3}{r_{min}^3}\rho^3\Big) \tag{12}$$

where $q_c = q(r = 0)$, r_{min} is the position of q_{min}, and $\Delta q = q_c - q_{min}$. The shape of the q profile is determined by adjusting the parameters q_{min}, Δq and r_{min}. Note that $|s|$ is proportional to Δq; therefore as Δq takes larger values the magnetic shear increases in both the $s < 0$ and $s > 0$ regions. A q profile compatible with experimental ones (see for example figure 10 in Ref. [20]) is presented in figure 1.
Toroidal magnetic field profile:

$$B_z = B_{z0}[1 + \delta(1 - \rho^2)]^{1/2}, \tag{13}$$

where B_{z0} is the vacuum magnetic field and the parameter δ is related to the magnetic properties of the plasma, i.e. for $\delta < 0$ the plasma is diamagnetic.

Gaussian-like ion poloidal velocity profile:

$$v_{i\theta} = 4v_{i\theta 0}\rho(1-\rho)\exp\Big(-\frac{(\rho-\rho_{min})^2}{h}\Big), \tag{14}$$

where the parameter $h > 0$ is related to the velocity shear, i.e. $|v'_{i\theta}|$ increases when h takes smaller values, and $v_{i\theta 0}$ defines the extremum of $v_{i\theta}$.
Either peaked on axis toroidal velocity profile:

$$v_{iz} = v_{iz0}(1-\rho^3)^3 \tag{15}$$

or Gaussian-like v_{iz} profile similar to that of (14); it is also noted that the results do not change if, alternative to (15), a peaked on axis toroidal velocity profile of the form

$$v_{iz} = v_{iz0}(1-\rho)\exp\left(-\frac{\rho^2}{h}\right)$$

is employed;
density profile:

$$n = n_0(1-\rho^3)^3. \tag{16}$$

In addition, the ion pressure can be expressed in terms of the total pressure by the relation

$$P_i = \lambda P \quad , \quad 0 < \lambda < 1 \ . \tag{17}$$

It is noted here that the free parameters q_0, q_{min}, r_{min}, $v_{i\theta 0}$, v_{iz0} and h aid in obtaining a variety of safety factor and velocity profiles consistent with those observed in tokamaks. An example showing q-profiles compatible with experimental ones measured in the tokamak JT-60U is given in Fig. 1 of Ref. [18].

Since in tokamaks $M_\theta < 0.1$, the convective flow term on the left hand side of (3) and therefore the flow term $M_\theta^2 B_\theta^2/r$ in (10) are perturbative around the "static" equilibrium $M_\theta^2 = 0$ and henceforth will be neglected. It should be noted, however, that this approximation may be not good for non-circular cylindrical or axisymmetric plasmas because in these cases the convective term in the momentum equation depends on the velocity shear which in certain regions may become large (see for example the z-independent cylindrical and axisymmetric incompressible MHD equilibrium equations (23) and (22) in Refs. [21] and [22] respectively). The following quantities then can be calculated self-consistently: the poloidal magnetic field, $B_\theta = \epsilon\rho B_z/q$, the magnetic shear $s = (r/q)(dq/dr)$, the current density via Ampére's law, the pressure by integration of (11) and setting $P(1) = 0$, the ion and electron pressures $P_i = \lambda P$ and $P_e = (1-\lambda)P$, the electric field by Eq. (9) for the ions

$$E_r(\rho) = \frac{1}{er_0 n(\rho)}\frac{dP_i(\rho)}{d\rho} + v_{iz}(\rho)B_\theta(\rho) - v_{i\theta}(\rho)B_z(\rho), \tag{18}$$

its shear $|E'_r|$ and $\omega_{E\times B}$ by (1). Also, the electron velocity components v_{ez} and $v_{e\theta}$ can be determined by the relation $\mathbf{J} = ne(\mathbf{v}_i - \mathbf{v}_e)$. It is noted here that the ∇P_i term in (18) can be obtained in the framework of the ideal Hall-MHD model, alternatively to the complete two fluid one, which includes the generalized Ohm's law:

$$\mathbf{E} + \mathbf{v}\times\mathbf{B} = \frac{1}{en}\left(\mathbf{J}\times\mathbf{B} - \nabla P_e\right). \tag{19}$$

Neglecting in the Hall-MHD momentum equation the convective flow term (which for the case under consideration corresponds to $M_\theta = 0$), the term $\mathbf{j} \times \mathbf{B}$ in (19) can be expressed in terms of the total pressure gradient:

$$\mathbf{J} \times \mathbf{B} = \nabla P = \nabla(P_i + P_e);$$

then Eq. (19) leads to (18). The above prescriptions and subsequent suggested calculations comprise a procedure to solve analytically the set of the two-fluid equations. The calculations have been performed analytically by developing a programm for symbolic computation [23] in connection with [24].

Inspection of (18) implies that in addition to the dependence of E_r and E_r' on the magnetic shear through the $dP_i/d\rho$ term, s is involved in the v_{iz} term through the q dependence of B_θ. The quantity $\omega_{\mathbf{E}\times\mathbf{B}}$ is stronger affected by the magnetic shear because s is involved in both the v_{iz} and $v_{i\theta}$ terms of $\omega_{\mathbf{E}\times\mathbf{B}}$ [see Eqs. (20) and (21) in section 3]. These observations indicate that there is a synergetic contribution of magnetic shear and flow to E_r, E_r', and $\omega_{\mathbf{E}\times\mathbf{B}}$. In this report results not obtainable within the framework of MHD will mainly be presented in the next section. MHD results were reported in Ref. [18].

3. Results

We have set the following values for some of the parameters: $B_{z0} = 1T$, $\delta = -0.0975$, $Z_i = 1$, $r_0 = 1m$, $R_0 = 3m$, $n_0 = 5 \times 10^{19} part./m^3$, $\lambda = 0.6$. The choice $q_{min} \geq 2$ was made because according to experimental evidence for $q_{min} < 2$ strong MHD activity destroys confinement possibly due to a double tearing mode [25]. A similar result was found numerically for one-dimensional cylindrical equilibria with hollow currents in [26]. Moreover in discharges with reversed magnetic shear in JET a correlation was found between the formation of ITBs and q_{min} reaching an integer value (2 or 3) [27]. The impact of the magnetic shear and flow profiles on the equilibrium characteristics was examined by varying the parameters Δq, q_{min}, r_{min}, h, v_{iz0} and $v_{i\theta 0}$ in the ranges (4-14), (2-3), (0.5-0.6), (0.001-0.1), (10^5-10^6 ms^{-1}) and (10^4-10^5 ms^{-1}) respectively in consistence with experimental regimes; consequently $q_c = q_{min} + \Delta q$ varies from 6 to 16 and it is guaranteed that $M_\theta^2 \approx M_z^2$, where $M_z^2 = [n(m_i v_{iz}^2 + m_e v_{ez}^2)]/B_z^2$, a scaling typical in tokamaks because $B_z \approx 10 B_\theta$ and $v_{iz} \approx 10 v_{i\theta}$ [28, 16]. The impact of the variation of magnetic shear through Δq was studied by keeping r_{min} and q_{min} constant, while the impact of r_{min} and q_{min} was examined with constant Δq.

First we will briefly report certain characteristics of the pressure and toroidal current density profiles which remain similar as in MHD. The total pressure profile, and therefore the P_i one, is peaked and for $s < 0$ becomes steeper when $|s|$ increases as can be deduced from Eq. (11) (see also figure 2). In addition (11) implies that the profile becomes steeper as the plasma becomes more diamagnetic, i.e. when B_z' in connection with δ in (13) takes larger values. The J_z-profile is hollow with its maximum located in the region where the q_{min} lies as can be seen in figure 3. These characteristics are observed in discharges with ITBs [11] and are favorable for ITB formation. Especially for $s > 2$ a reversal of J_z occurs in the $s > 0$ region. This characteristic is discussed further in Ref. [18]. It is also noted that a sufficient stability criterion for equilibria with reversed current density in the outer plasma area and monotonically increasing q-profiles was derived in Ref. [29].

The conclusions on the impact of the magnetic shear and flow on E_r, $|E_r'|$ and $\omega_{\mathbf{E}\times\mathbf{B}}$ are reported on an individual basis in the rest of this section.

3.1 Electric field (E_r)

1. The electric field consists of the ∇P_i, v_{iz} and, $v_{i\theta}$ contributions in connection with the first, second, and third term in Eq. (18). Each of these terms contributes of about the same order of magnitude to E_r (figure 4). This is consistent with experimental evidence [11]. A similar result was obtained in a different way in [30] (see figure 4 therein). It is apparent from (18) that E_r depends linearly on v_{iz} and $v_{i\theta}$ with the overall velocity contribution to E_r, however, depending on the relative signs of v_{iz}, $v_{i\theta}$ and B_z.

2. Typical E_r profiles exhibit an extremum located in the neighborhood of the q_{min} position (figure 4).

3. Increase of $|s|$, by increasing Δq, makes the maximum of $|E_r|$ to take larger values (figure 5). Depending on the direction (toroidal or poloidal) of the velocity and the shape of its profile, variation of Δq from 4 to 14 increases the values of the $|E_r|$ maximum in a range that varies from 5.6% for purely poloidal flow to 48% for purely peaked toroidal flow. It is reminded that, in addition to the s dependence of the ∇P_i term in (18), s contributes to E_r synergetically with the v_{iz} term (the $v_{i\theta}$ term is s independent).

4. The larger r_{min} the higher the values of the $|E_r|$ maximum (for given values of Δq and q_{min}) as shown in figure 6. Quantitatively for a variation of r_{min} from 0.5 to 0.6, the increase of $|E_r|$ maximum varies from 36% to 70%. Also the position of the extremum (located in the vicinity of r_{min}) is displaced outwards.

5. The larger q_{min} the smaller the $|E_r|$ maximum (figure 7). In particular, increase of q_{min} from 2 to 3 (with $\Delta q = 4$ and $r_{min} = 0.5$), results in a decrease of the $|E_r|$ maximum in the range (12-40)%.

6. When the flow shear increases (by decreasing h from 0.1 to 0.001) the extremum of E_r remains practically unchanged in most of the cases considered.

3.1 Shear of the electric field ($|E_r'|$)

1. As in the case of E_r the contributions from the ∇P_i-, v_{iz}- and $v_{i\theta}$-related terms to E_r' are of the same order of magnitude as shown in figure 8.

2. The profile of E_r' exhibits one local extremum on each side of the q_{min} position (figure 9). The two extrema are of opposite sign.

3. Increase of $|s|$ increases both maxima of $|E_r'|$ in most of the flow cases considered and this increase is larger in the region where $s > 0$ than that where $s < 0$. This is shown in figure (9). For certain combinations of the velocity components, however, the one extremum increases and the other decreases. Such a case with peaked toroidal v_{iz} and poloidal $v_{i\theta}$ flow is shown in figure 10.

4. The larger r_{min} the higher the maxima of $|E_r'|$ (figure 11) unless the case of poloidal velocity in conjunction with Gaussian-like toroidal one. Depending on the direction and the shape of the velocity this increase varies from from 8% to 42%. Also the profile of $|E_r'|$ is displaced outwards as can be seen in figure 11.

5. An increase of q_{min} results in a decrease of the $|E_r'|$ extremum in the $s > 0$ region in all of the cases considered while in the $s < 0$ region this happens for $v_{i\theta} = 0$ (figure 12).

6. By increasing the velocity shear the maxima of $|E_r'|$ are also increased in all the cases considered (figure 13).

7. For either purely toroidal or poloidal flow, increase of the maximum absolute value of the velocity by a factor increases the maxima of $|E_r'|$ by the same factor in all of the cases considered with the following exception: purely toroidal peaked flow for which the maximum in the $s < 0$ region increases and the one in the $s > 0$ region decreases.

8. For either purely toroidal or purely poloidal flow, inversion of the velocity direction causes a change in the sign of the two E_r' extrema. Also, this inversion leads to (i) an increase of both maxima of $|E_r'|$ for Gaussian-like v_{iz}, (ii) an increase of the one $|E_r'|$ maximum in the $s > 0$ and a decrease of the other in the $s < 0$ region for peaked toroidal velocity and (iii) a decrease of both maxima for purely poloidal flow. For peaked v_{iz} the increase of the one $|E_r'|$-maximum in the $s > 0$ region caused by inversion is greater than the increase of the other in the $s < 0$ region.

3.3 Shear of the $\mathbf{E} \times \mathbf{B}$ *velocity* ($\omega_{\mathbf{E}\times\mathbf{B}}$)

1. The profile of $\omega_{\mathbf{E}\times\mathbf{B}}$ (Eq. 1) possesses two maxima, one in the region with $s < 0$ and one located in the region with $s > 0$ (figure 14). Larger of the two maxima is the one which lies in the region of steeper pressure profile.

2. The impact of the magnetic shear on $\omega_{\mathbf{E}\times\mathbf{B}}$ is stronger than that in MHD due to the ∇P_i term of the electric field [Eq. (18)]. Specifically for constant B_z and arbitrary profiles of q, v_{iz} and $v_{i\theta}$, Eq. (1) yields at the point where $E_r' = 0$

$$\omega_{\mathbf{E}\times\mathbf{B}} = \Big|\lambda \frac{(1-s)(2-s)B_z\rho\epsilon}{enqr_0^2(\rho^2 + \frac{q^2}{\epsilon^2})} - \omega_{\mathbf{E}\times\mathbf{B}-MHD}\Big|, \tag{20}$$

where

$$\omega_{\mathbf{E}\times\mathbf{B}-MHD} = \frac{(1-s)\big(\frac{\epsilon\rho v_{iz}}{q} - v_{i\theta}\big)}{r_0^2\big(\rho^2 + \frac{q^2}{\epsilon^2}\big)} \tag{21}$$

The first term in (20) stems from the ∇P_i part of E_r in (11) while the second term comes from the v_{iz} and $v_{i\theta}$ parts of E_r. The subscript MHD is used to emphasize the similarity of (21) with the respective MHD relation derived in Ref. [18] [equation (18) therein]. It is apparent that the ∇P_i-related dependence of $\omega_{\mathbf{E}\times\mathbf{B}}$ on s, proportional to $(1-s)(2-s)$, is stronger than the v_{iz} and $v_{i\theta}$ dependence proportional to $1-s$; also, the absolute values of the ∇P_i-, v_{iz}- and $v_{i\theta}$- related

terms are individually larger for $s < 0$ than $s > 0$. The contribution of each of these terms to $\omega_{\mathbf{E}\times\mathbf{B}}$ however is of the same order of magnitude. Note that despite of the tokamak pertinent scaling $v_{iz} \approx 10 v_{i\theta}$, the contributions of v_{iz} and $v_{i\theta}$ terms are of the same order of magnitude because of the factor $\epsilon\rho/q$. In connection with this result we may note here a conclusion in Ref. [12] that suppression of turbulence in association with flute-like fluctuations caused by the $\mathbf{E} \times \mathbf{B}$ shear occurs regardless of the rotation direction. The "equipartition" of the three terms holds in general for the whole $\omega_{\mathbf{E}\times\mathbf{B}}$ profile obtained via the symbolic computation programme as shown in Fig 15.

3. Increase of the flow via either $|v_{iz0}|$ or $|v_{i\theta 0}|$ by a factor increases the maxima of $\omega_{\mathbf{E}\times\mathbf{B}}$ by the same factor.

The impact of the magnetic shear through Δq and the flow on $\omega_{\mathbf{E}\times\mathbf{B}}$ is similar as that on E_r'. Specifically:

1. Increase of $|s|$ leads to larger values for the maxima of $\omega_{\mathbf{E}\times\mathbf{B}}$ in most of the flow cases considered (figure 16). There are some combinations of velocity components however for which the one maximum increases and the other decreases. Such a case is shown in figure 17. In which region ($s < 0$ or $s < 0$) the increase takes place depends on the particular velocity components involved and the shape of the toroidal velocity profile.

2. The larger r_{min} the greater the $\omega_{\mathbf{E}\times\mathbf{B}}$-maxima (figure 18) in the same cases as for E_r'. The profile of $\omega_{\mathbf{E}\times\mathbf{B}}$ is also displaced outwards as can be seen in figure 18.

3. Increase of q_{min} causes (i) a decrease of the $\omega_{\mathbf{E}\times\mathbf{B}}$-maximum in the $s > 0$ region in all of the cases considered and (ii) an increase of $\omega_{\mathbf{E}\times\mathbf{B}}$ -maximum in the $s < 0$ one for $v_{i\theta} \neq 0$ (figure 19).

4. The larger the flow shear the greater the $\omega_{\mathbf{E}\times\mathbf{B}}$ maxima in all of the cases considered (figure 20).

5. $\omega_{\mathbf{E}\times\mathbf{B}}$ is affected by the relative signs of $v_{i\theta}$, v_{iz} and B_z as is apparent from Eqs. (20) and (21). In particular (i) inversion of the Gaussian-like toroidal velocity increases the maxima of $\omega_{\mathbf{E}\times\mathbf{B}}$ (figure 21), (ii) the maximum of $\omega_{\mathbf{E}\times\mathbf{B}}$ in the $s > 0$ region increases while the one in the $s < 0$ region decreases due to the reversal of the peaked toroidal velocity and (iii) they decrease by inversion of the poloidal velocity. Finally for both Gaussian-like velocity components the variation caused by inversion is greater in the $s > 0$ region.

4. Summary and Conclusions

In this report tokamak equilibria with reversed magnetic shear and sheared flow have been studied within the framework of two-fluid model in the limit of infinite aspect ratio. The study is based on a slightly reduced set of two-fluid equations in which the electron momentum equation is replaced by the respective MHD one. Neglecting the flow term in this equation (because in cylindrical geometry it is small for tokamaks) and prescribing

the profiles of six free quantities in accord with ITB experimental ones, i.e. the toroidal magnetic field B_z, the safety factor q, the toroidal and poloidal ion velocities v_{iz} and $v_{i\theta}$, the density n [Eqs. (13)-(16)] and the ion pressure in terms of the total pressure, $P_i = \lambda P$, we have constructed analytic solutions in calculating self consistently the following quantities: P [and therefore P_i and the electron pressure $P_e = (1-\lambda)P$], the current density and the radial electric field E_r; the electric field shear, $|E_r'|$, and the shear of the $\mathbf{E}\times\mathbf{B}$-velocity, $\omega_{\mathbf{E}\times\mathbf{B}}$ [Eq. (1)] have also been calculated. Gaussian-like profiles for $v_{i\theta}$ and either Gaussian-like or peaked-on-axis ones for v_{iz} have been considered. In addition, for reversed magnetic shear profiles the impact of s and the flow on the equilibrium characteristics has been examined by varying the parameters Δq which $|s|$ is proportional to, the minimum of q, q_{min}, its position, r_{min}, the extrema of the velocity components, v_{iz0} and $v_{i\theta 0}$, and a parameter h which decreases with increasing velocity shear. The results are as follows.

1. The pressure profiles become steeper in the region of $s < 0$.

2. The profile of the toroidal current density J_z is hollow and a reversal occurs in the outer plasma region for $s > 2$ in connection with appropriate values of Δq.

3. The $|E_r|$ profile has a maximum located close to the q_{min} position while the $|E_r'|$ and $\omega_{\mathbf{E}\times\mathbf{B}}$ ones have two local maxima the one in the $s > 0$ and the other in the $s < 0$ regions.

4. The contributions associated with ∇P_i, v_{iz}, and $v_{i\theta}$ to E_r, E_r' and $\omega_{\mathbf{E}\times\mathbf{B}}$ (the ∇P_i contribution being missed in MHD) are of the same order of magnitude.

5. The magnetic shear affects E_r and E_r' explicitly through ∇P_i and implicitly in conjunction with v_{iz}; s has an additional impact on $\omega_{\mathbf{E}\times\mathbf{B}}$ in connection with $v_{i\theta}$. The explicit impact of s is stronger; in particular for B_z =constant, the ∇P_i contribution to $\omega_{\mathbf{E}\times\mathbf{B}}$ at the point where $E_r' = 0$ is proportional to $(1-s)(2-s)$ [Eq. (20)] while the contribution through the flow terms is proportional to (1-s) [Eq. (21)].

6. Increase of $|s|$ results in an increase in the maximum of $|E_r|$ in all of the cases considered. Also, the maxima of $|E_r'|$ and $\omega_{\mathbf{E}\times\mathbf{B}}$ increase in most of the flow cases considered. When either the toroidal and poloidal velocity contributions cancel each other or the velocity is purely toroidal peaked, the increase is greater in the $s > 0$ region. Also pending on the direction and shape of the flow, the increase varies from 56.4% to 323%.

7. The larger r_{min} the greater the maxima of $|E_r|$, $|E_r'|$, and $\omega_{\mathbf{E}\times\mathbf{B}}$.

8. The larger q_{min} the smaller the maximum of $|E_r|$ but the larger the maxima of $|E_r'|$ and $\omega_{\mathbf{E}\times\mathbf{B}}$ in the $s > 0$ region.

9. Stronger flow, by larger values of $|v_{iz0}|$ and $|v_{i\theta 0}|$, leads to linear increase in E_r, $|E_r'|$, and $\omega_{\mathbf{E}\times\mathbf{B}}$.

10. The larger the flow shear (by smaller values of the parameter h) the slightly smaller the maximum of $|E_r|$ but the larger the maxima of $|E_r'|$ and $\omega_{\mathbf{E}\times\mathbf{B}}$.

11. E_r, E_r', and $\omega_{\mathbf{E}\times\mathbf{B}}$ are sensitive to the relative signs of v_{iz}, $v_{i\theta}$, and B_z.

In summary, alike MHD, in the framework of two-fluid model the magnetic shear and sheared flow (toroidal and poloidal) act synergetically on E_r, E_r', and $\omega_{\mathbf{E}\times\mathbf{B}}$ which may play a role in the formation of ITBs. However the impact of magnetic shear on these quantities is stronger than that in MHD due to the additional ∇P_i contribution to the aforementioned terms.

Acknowledgements

Part of this work was conducted during a visit of the authors G.P. and G.N.T. to the Max-Planck-Institut für Plasmaphysik, Garching. The hospitality of that Institute is greatly appreciated.

This work was performed under the Contract of Association ERB 5005 CT 99 0100 between the European Atomic Energy Community and the Hellenic Republic.

References

[1] Gruber, O. it et al 2000 Plasma Phys. Control. Fusion **44** A117.

[2] Zohm, H. *et al* 2003 Nucl. Fusion **43** 1570.

[3] Ide, S. *et al* 1996 Plasma Phys. Control. Fusion **38** 1645.

[4] Litaudon, X. *et al* 1996 Plasma Phys. Control. Fusion **38** 1603.

[5] Litaudon, X. *et al* 2003 Nucl. Fusion **43** 565.

[6] Strait, E.J. *et al* 1995 Phys. Rev. Lett. **75** 4421.

[7] Conway, G.D. *et al* 2001 Plasma Phys. Control. Fusion **43** 1239.

[8] Levinton, F.M., *et al* 1995 Phys. Rev. Lett. **75** 4417.

[9] Tala, T.J.J. *et al* 2001 Plasma Phys. Control. Fusion **43** 507.

[10] Candy, R. and Waltz, R.E. 2003 Phys. Rev. Lett. **91** 045001.

[11] Connor, J.W. *et al* 2004 Nucl. Fusion **44** R1.

[12] Hahm T.S., Burrell, K.H. 1995 Phys. Plasmas **2** 1648.

[13] Waltz, R.E. *et al* 1997 Phys. Plasmas **2** 24892.

[14] Crisanti, F. *et al* 2001 Nucl. Fusion **41** 883.

[15] Crobé, K *et al* 2005 Phys. Rev. Lett. **95** 155003.

[16] Bell, R. E. *et al* 1998 Phys. Rev. Lett. **7** 1429.

[17] Bell, M. G. *et al* 1999 Plasma Phys. Control. Fusion **41** A719.

[18] Poulipoulis, G., Throumoulopoulos, G. N., Tasso, H. 2004 Plasma Phys. Control. Fusion **46** 639.

[19] Wolf, R. C. 2003 Plasma Phys. Control. Fusion **45** R1.

[20] Koide, Y. and the JT-60 Team 1997 Phys. Plasmas **4** 1623.

[21] Throumoulopoulos, G. N. and Tasso, H. 1997 Phys. Plasmas **4** 1492.

[22] Tasso, H. and Throumoulopoulos, G. N. 1998 Phys. Plasmas **5** 2378.

[23] The programme is available uppon request to the first author (G.P.)

[24] Wolfram Research, Mathematica, version 4.1; S. Wolfram, *The Mathematica book, 4^{th} ed.*, (Wolfram Media/Cambridge University Press, 1999).

[25] Wolf, R.C. *et al* 2000 Phys. Plasmas **7** 1839.

[26] Kerner, W. and Tasso, H. 1982 Plasma Physics **24** 97.

[27] Joffrin, E. *et al* 2002 Plasma Phys. Control. Fusion **44** 1739.

[28] Meister, H. *et al* 2001 Nuclear Fusion **41** 1633.

[29] Lortz, D. and Zeiler, A. 1994 Phys. Plasmas **1** 670.

[30] Zhu, P., Horton, W. and Sugama, H. 1999 Phys. Plasmas **6** 2503.

Figure captions

Figure 1: Safety factor profile in connection with Eq. (12) compatible with the experimental one measured in JT-60U [20] (figure 10 therein).

Figure 2: Pressure profiles for two values of the reversed-magnetic-shear parameter Δq normalized with respect to the value of P at the magnetic axis.

Figure 3: Toroidal current density profiles for two values of Δq which show the hollow shape and the reversal in the outer plasma region. The profiles are normalized with respect to the maximum of J_z for $\Delta q = 4$.

Figure 4: Profiles of the ∇P_i, v_{iz} and $v_{i\theta}$ contributions to the electric field, E_r, showing that all three contributions are of the same order of magnitude. The v_{iz} profile is peaked on axis. The profiles are normalized with respect to the extremum of ∇P_i contribution.

Figure 5: Increase of the normalized absolute value of the electric field extremum due to the variation of Δq for $q_{min} = 4$, $r_{min} = 0.5$, Gaussian-like v_{iz} profile and $v_{i\theta} = 0$.

Figure 6: Increase of the absolute value of the E_r extremum when the distance r_{min} in connection with the q_{min} position becomes larger. Also, the position of the extremum is displaced outwards. Here, $q_{min} = 2$, $\Delta q = 4$, and the flow is purely toroidal peaked on axis. The profiles are normalized with respect to the extremum for $r_{min} = 0.5$.

Figure 7: Decrease of the normalized $|E_r|$ maximum when q_{min} increases for $\Delta q = 4$, $r_{min} = 0.5$, peaked v_{iz} and Gaussian-like localized $v_{i\theta}$ ($h = 0.001$).

Figure 8: Profiles of the ∇P_i, v_{iz} and $v_{i\theta}$ contributions to the electric field shear, E_r', showing that all three contributions are of the same order of magnitude. The v_{iz} profile is peaked on axis. The profiles are normalized with respect to the extremum of the ∇P_i contribution in the $s < 0$ region.

Figure 9: Increase of the normalized $|E_r'|$ maxima caused by an increase of the magnetic shear in connection with variation of Δq. The plots were obtained for v_{iz} peaked and $v_{i\theta} = 0$.

Figure 10: Increase of the $|E_r'|$ extremum in the $s > 0$ region due to the increase of Δq. The profiles are obtained for v_{iz} peaked and $v_{i\theta} \neq 0$ and are normalized with respect to the value of the extremum in the $s < 0$ region for $\Delta q = 4$.

Figure 11: Increase of the $|E_r'|$ extrema as r_{min} takes larger values for $q_{min} = 2$, $\Delta q = 4$, and peaked purely toroidal flow. Also the positions of the extrema are displaced outwards. The profiles are normalized with respect to the E_r' extremum for $r_{min} = 0.5$

Figure 12: Decrease of the $|E_r'|$ extremum in the $s < 0$ region for purely toroidal Gaussian-like flow due to the increase of q_{min}. For this particular case of flow the variation of the other extremum in the $s > 0$ region is negligible.

Figure 13: Increase of the $|E_r'|$ extrema due to the increase of the flow shear for Gaussian-like v_{iz} and $v_{i\theta} = 0$.

Figure 14: A typical $\omega_{\mathbf{E}\times\mathbf{B}}$ profile for purely poloidal flow, normalized with respect to the maximum value in the $s > 0$ region.

Figure 15: Profiles of the ∇P_i, v_{iz} and $v_{i\theta}$ contributions to $\omega_{\mathbf{E}\times\mathbf{B}}$ showing that all three are of the same order of magnitude. The v_{iz} profile is peaked on axis. The normalization is made with respect to the maximum value of the ∇P_i contribution in the $s < 0$ region.

Figure 16: Increase of the normalized $\omega_{\mathbf{E}\times\mathbf{B}}$ maxima due to the increase of the magnetic shear. Both velocity components have Gaussian-like profiles.

Figure 17: Increase of the $\omega_{\mathbf{E}\times\mathbf{B}}$ extremum in the $s < 0$ and decrease in the $s > 0$ regions due to the increase of Δq. The profiles are obtained for v_{iz} Gaussian-like and $v_{i\theta} = 0$ and are normalized with respect to the $s < 0$ extremum of $\omega_{\mathbf{E}\times\mathbf{B}}$ for $\Delta q = 4$.

Figure 18: Increase of the normalized $\omega_{\mathbf{E}\times\mathbf{B}}$ maxima due to the outward shift of the position of q_{min} for purely toroidal Gaussian-like flow.

Figure 19: Increase of the $\omega_{\mathbf{E}\times\mathbf{B}}$-extrema as q_{min} takes larger values when both velocity components have Gaussian-like profiles. In this particular case the increase of the extremum in the $s > 0$ region is very small. The profiles are normalized with respect to the $s > 0$ maximum of $\omega_{\mathbf{E}\times\mathbf{B}}$ for $q_{min} = 3$.

Figure 20: Increase of the $\omega_{\mathbf{E}\times\mathbf{B}}$ extrema caused by the increase of the flow shear for v_{iz} peaked and $v_{i\theta} \neq 0$. The normalization is made with respect to the $\omega_{\mathbf{E}\times\mathbf{B}}$ extremum in the $s > 0$ region for $h = 0.1$.

Figure 21: Increase of the normalized $\omega_{\mathbf{E}\times\mathbf{B}}$-extrema caused by inversion of a Gaussian-like toroidal velocity.

List of Figures

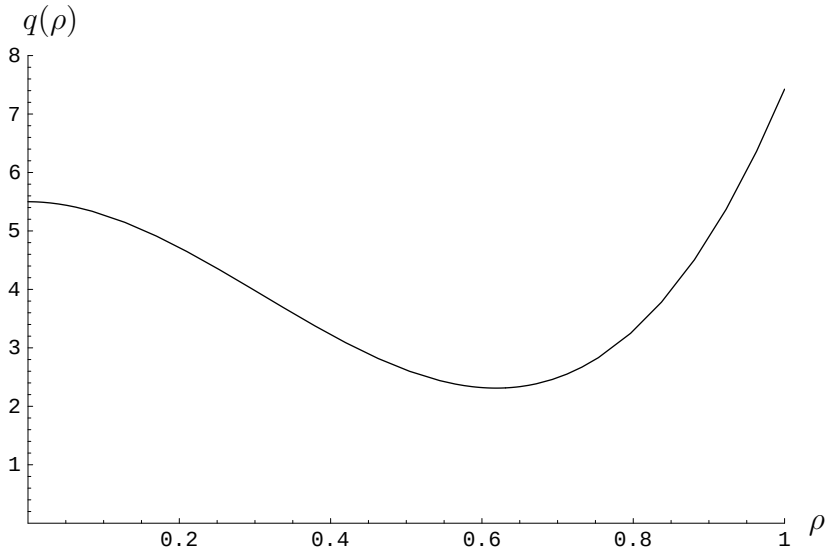

Figure 1: Safety factor profile in connection with Eq. (12) compatible with the experimental one measured in JT-60U [20] (figure 10 therein).

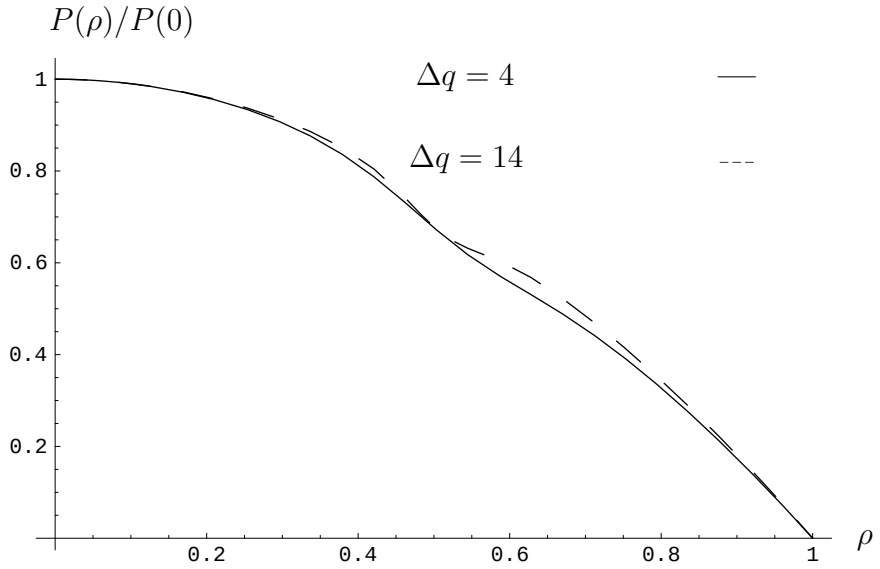

Figure 2: Pressure profiles for two values of the reversed-magnetic-shear parameter Δq normalized with respect to the value of P at the magnetic axis.

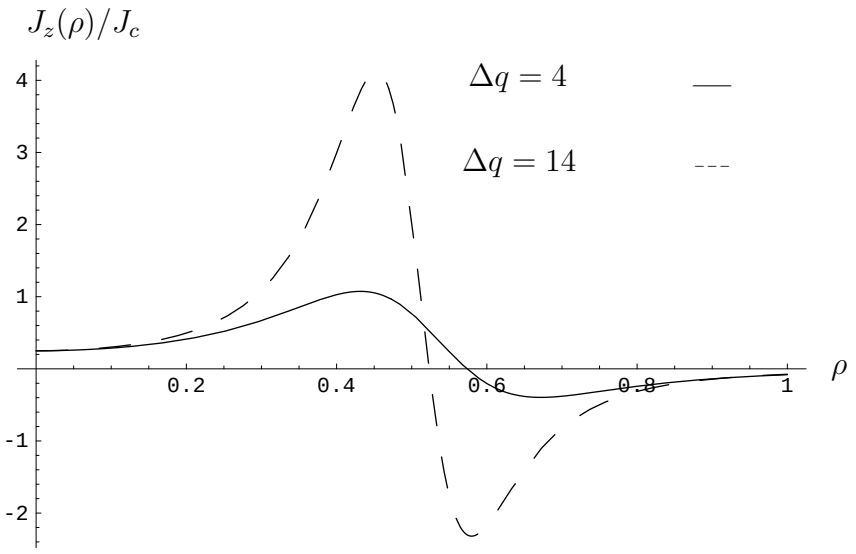

Figure 3: Toroidal current density profiles for two values of Δq which show the hollow shape and the reversal in the outer plasma region. The profiles are normalized with respect to the maximum of J_z for $\Delta q = 4$.

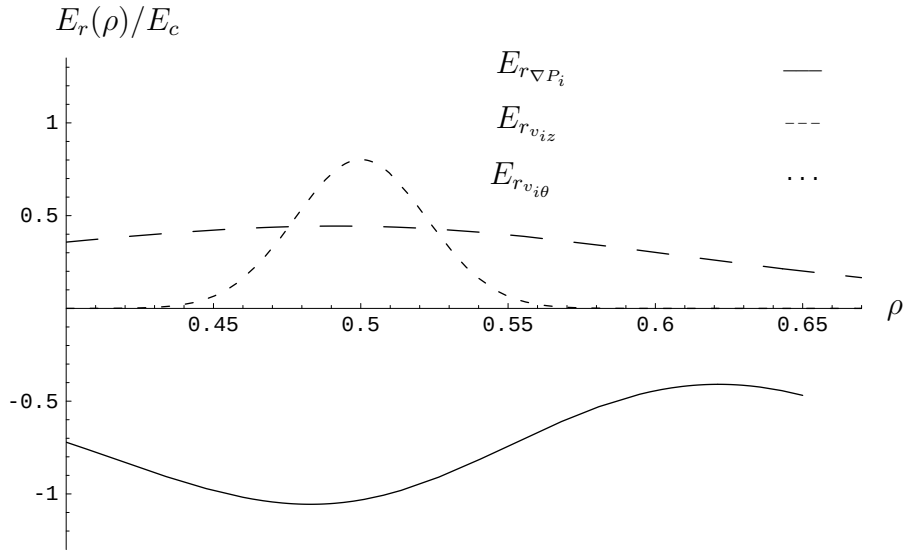

Figure 4: Profiles of the ∇P_i, v_{iz} and $v_{i\theta}$ contributions to the electric field, E_r, showing that all three contributions are of the same order of magnitude. The v_{iz} profile is peaked on axis. The profiles are normalized with respect to the extremum of ∇P_i contribution.

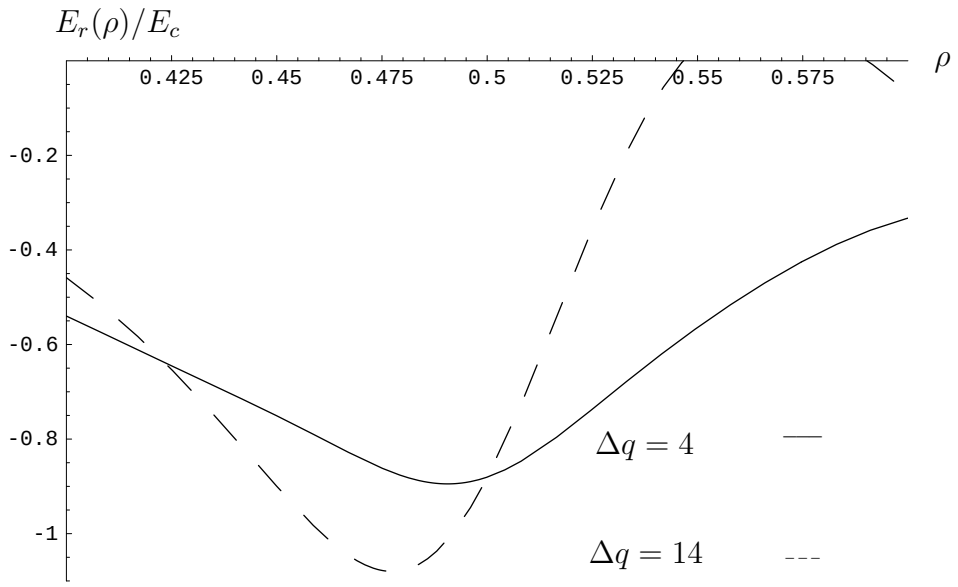

Figure 5: Increase of the normalized absolute value of the electric field extremum due to the variation of Δq for $q_{min} = 4$, $r_{min} = 0.5$, Gaussian-like v_{iz} profile and $v_{i\theta} = 0$.

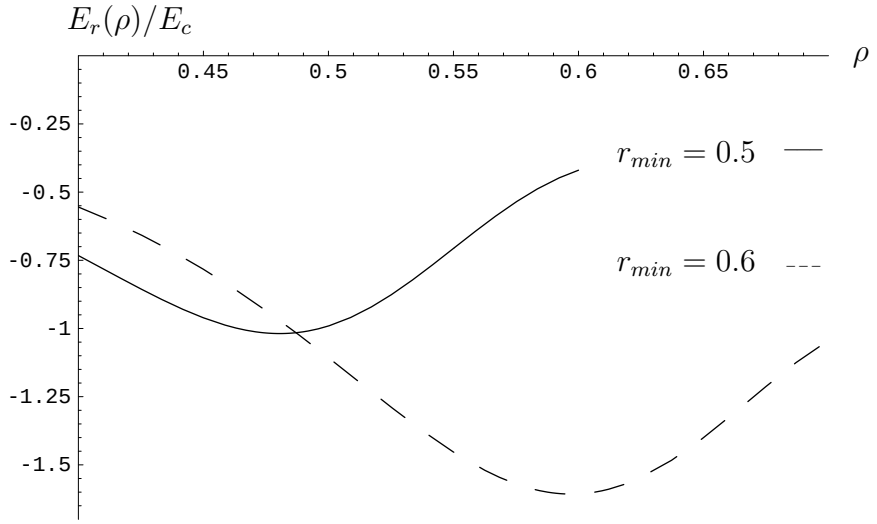

Figure 6: Increase of the absolute value of the E_r extremum when the distance r_{min} in connection with the q_{min} position becomes larger. Also, the position of the extremum is displaced outwards. Here, $q_{min} = 2$, $\Delta q = 4$, and the flow is purely toroidal peaked on axis. The profiles are normalized with respect to the extremum for $r_{min} = 0.5$.

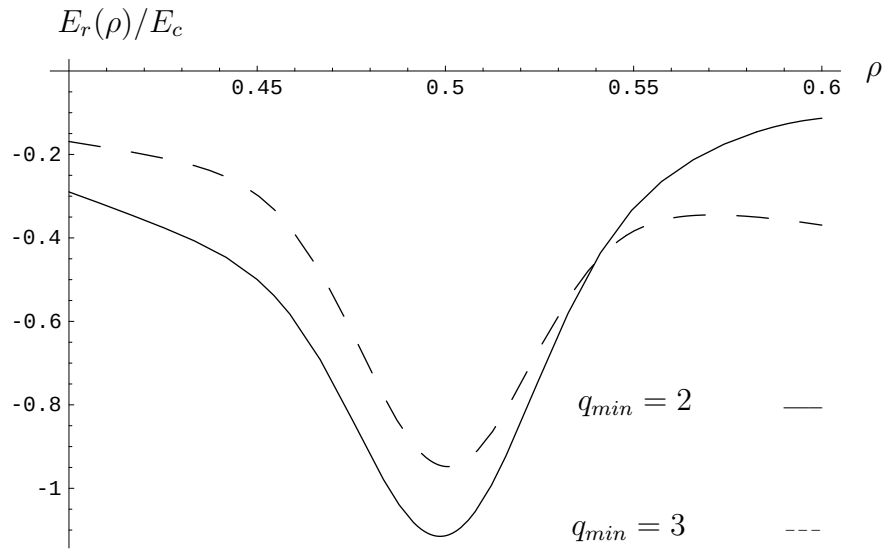

Figure 7: Decrease of the normalized $|E_r|$ maximum when q_{min} increases for $\Delta q = 4$, $r_{min} = 0.5$, peaked v_{iz} and Gaussian-like localized $v_{i\theta}$ ($h = 0.001$).

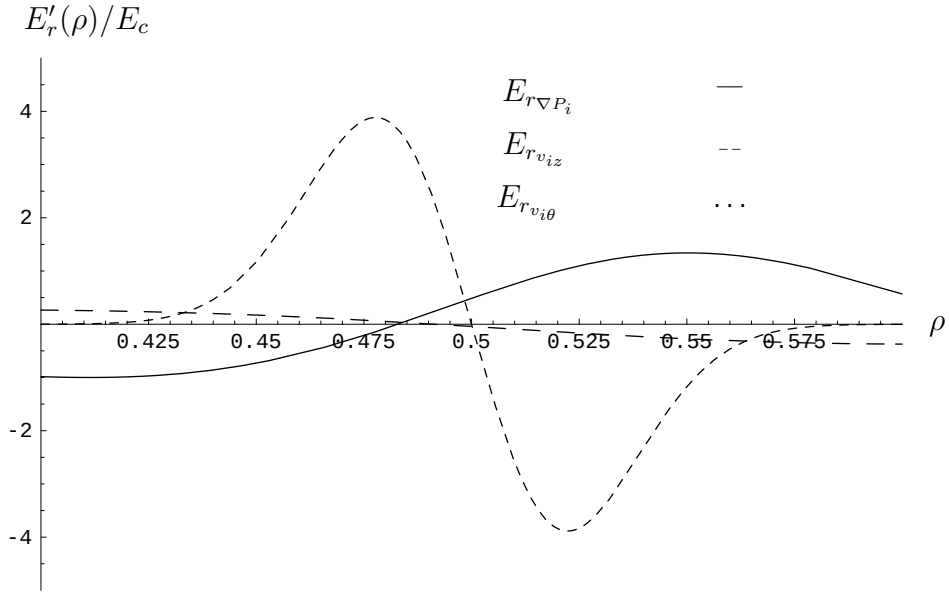

Figure 8: Profiles of the ∇P_i, v_{iz} and $v_{i\theta}$ contributions to the electric field shear, E'_r, showing that all three contributions are of the same order of magnitude. The v_{iz} profile is peaked on axis. The profiles are normalized with respect to the extremum of the ∇P_i contribution in the $s < 0$ region.

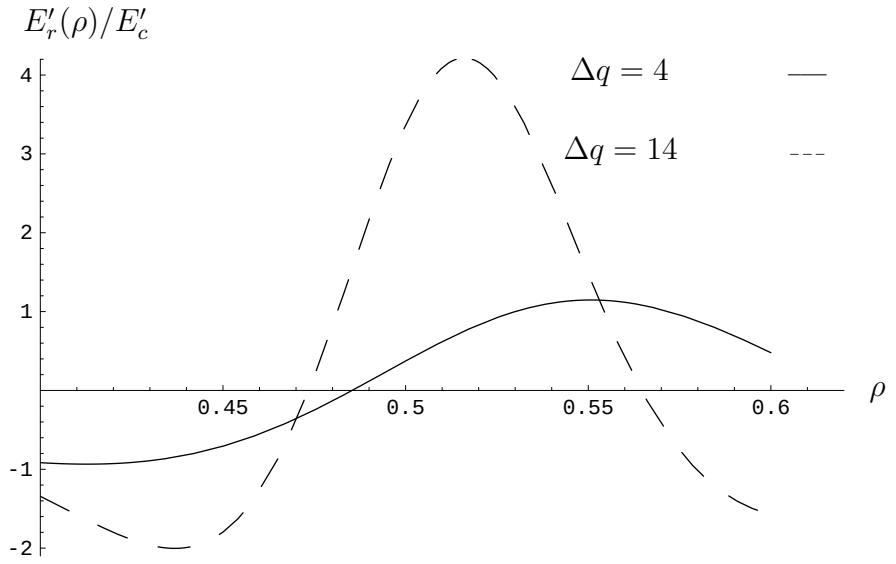

Figure 9: Increase of the normalized $|E_r'|$ maxima caused by an increase of the magnetic shear in connection with variation of Δq. The plots were obtained for v_{iz} peaked and $v_{i\theta} = 0$.

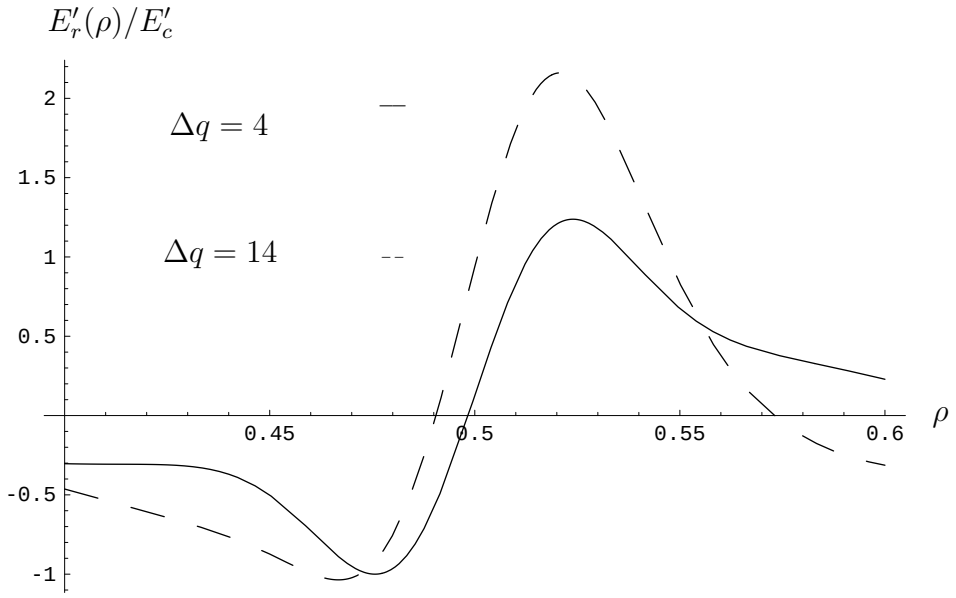

Figure 10: Increase of the $|E_r'|$ extremum in the $s > 0$ region due to the increase of Δq. The profiles are obtained for v_{iz} peaked and $v_{i\theta} \neq 0$ and are normalized with respect to the value of the extremum in the $s < 0$ region for $\Delta q = 4$.

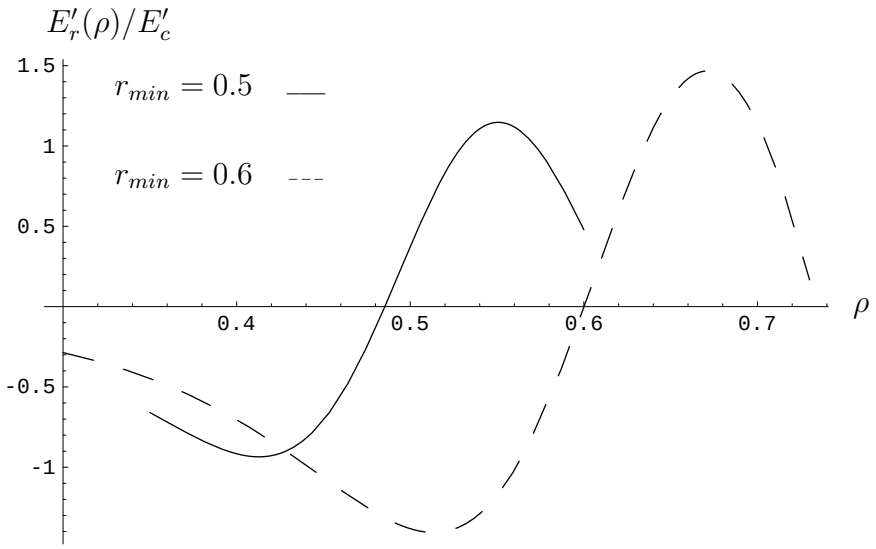

Figure 11: Increase of the $|E'_r|$ extrema as r_{min} takes larger values for $q_{min} = 2$, $\Delta q = 4$, and peaked purely toroidal flow. Also the positions of the extrema are displaced outwards. The profiles are normalized with respect to the E'_r extremum for $r_{min} = 0.5$.

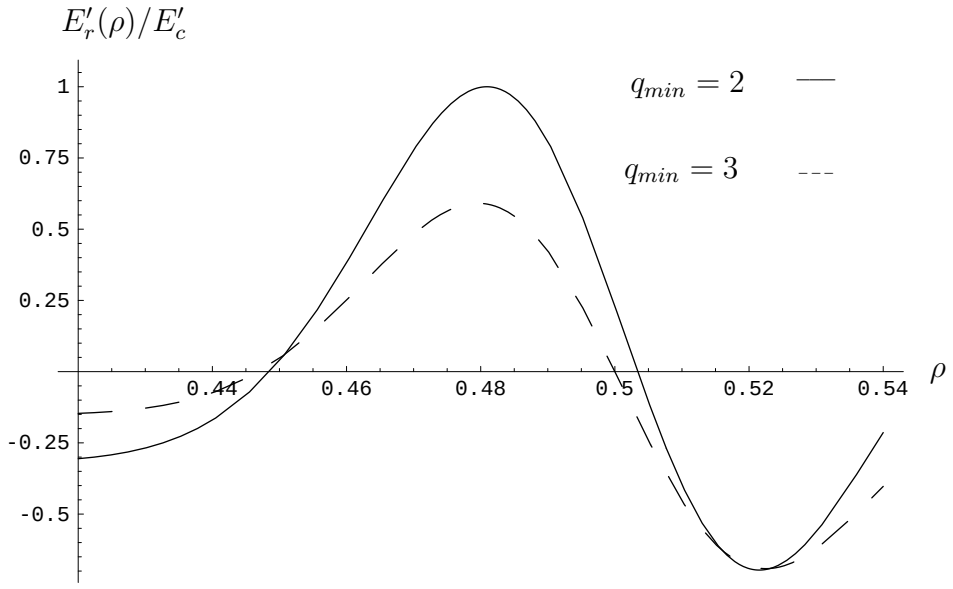

Figure 12: Decrease of the $|E'_r|$ extremum in the $s < 0$ region for purely toroidal Gaussian-like flow due to the increase of q_{min}. For this particular case of flow the variation of the other extremum in the $s > 0$ region is negligible.

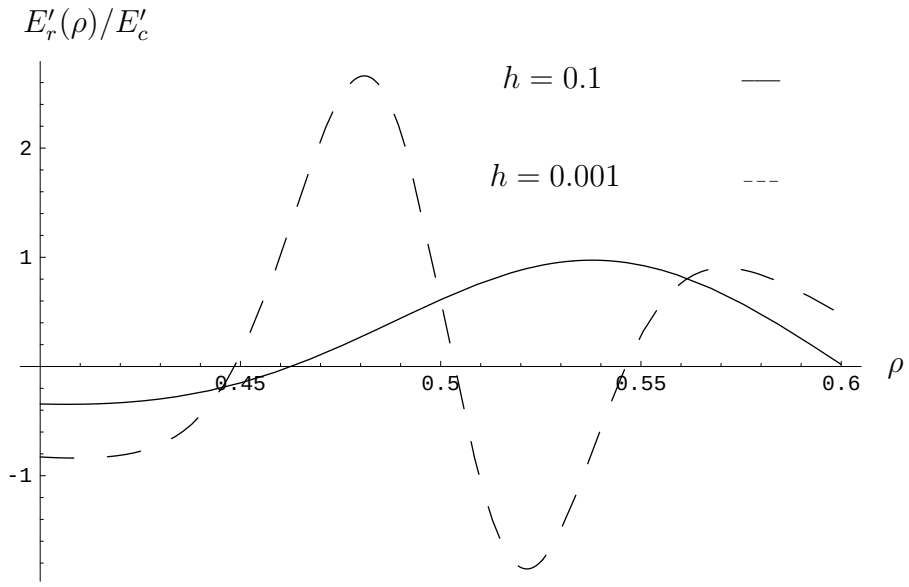

Figure 13: Increase of the $|E'_r|$ extrema due to the increase of the flow shear for Gaussian-like v_{iz} and $v_{i\theta} = 0$. The profiles are normalized with respect to the extremum in the $s > 0$ region for $h = 0.001$.

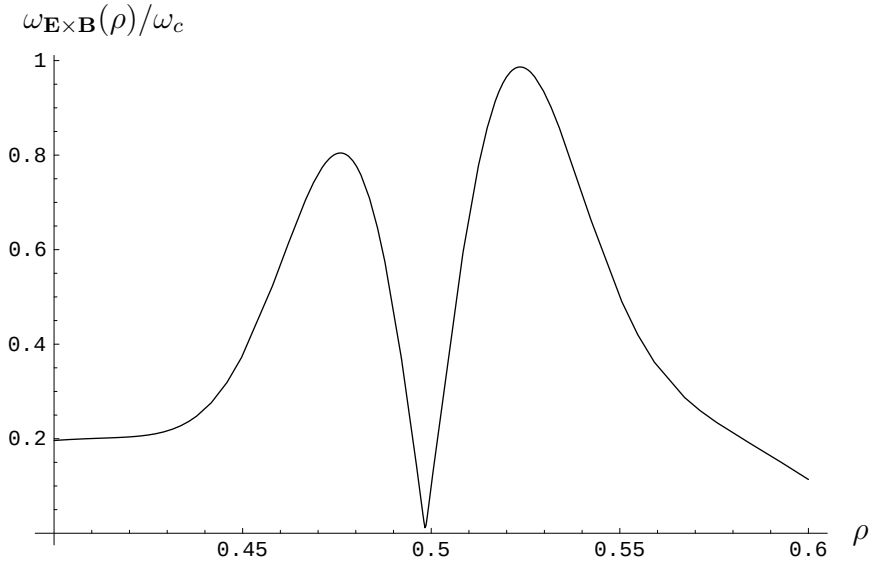

Figure 14: A typical $\omega_{\mathbf{E}\times\mathbf{B}}$ profile for purely poloidal flow, normalized with respect to the maximum value in the $s > 0$ region.

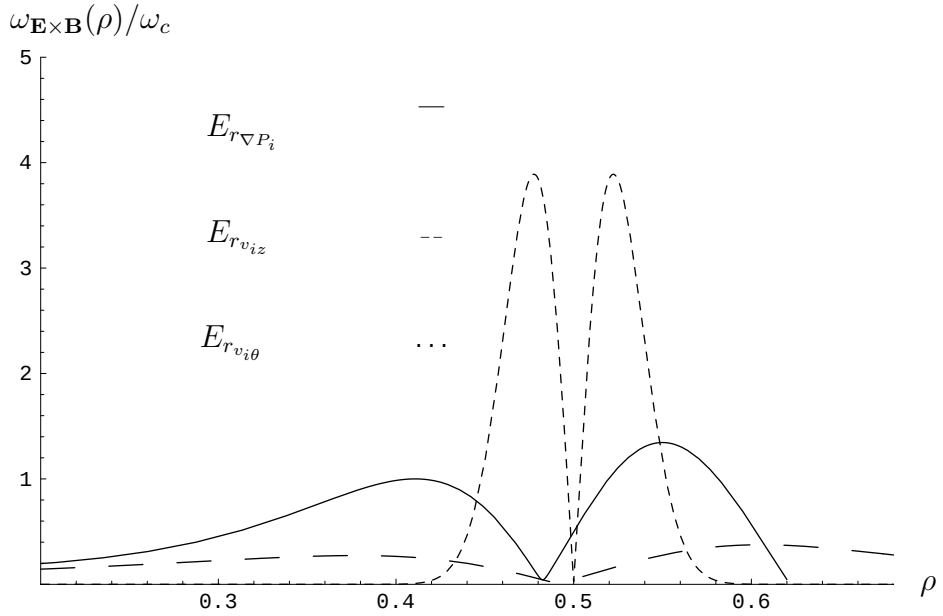

Figure 15: Profiles of the ∇P_i, v_{iz} and $v_{i\theta}$ contributions to $\omega_{\mathbf{E}\times\mathbf{B}}$ showing that all three are of the same order of magnitude. The v_{iz} profile is peaked on axis. The normalization is made with respect to the maximum value of the ∇P_i contribution in the $s < 0$ region.

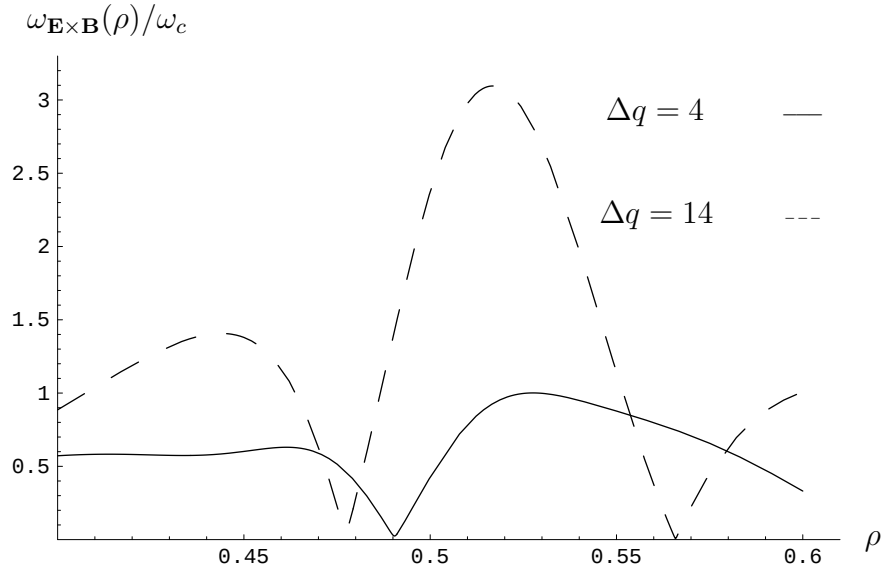

Figure 16: Increase of the normalized $\omega_{\mathbf{E}\times\mathbf{B}}$ maxima due to the increase of the magnetic shear. Both velocity components have Gaussian-like profiles.

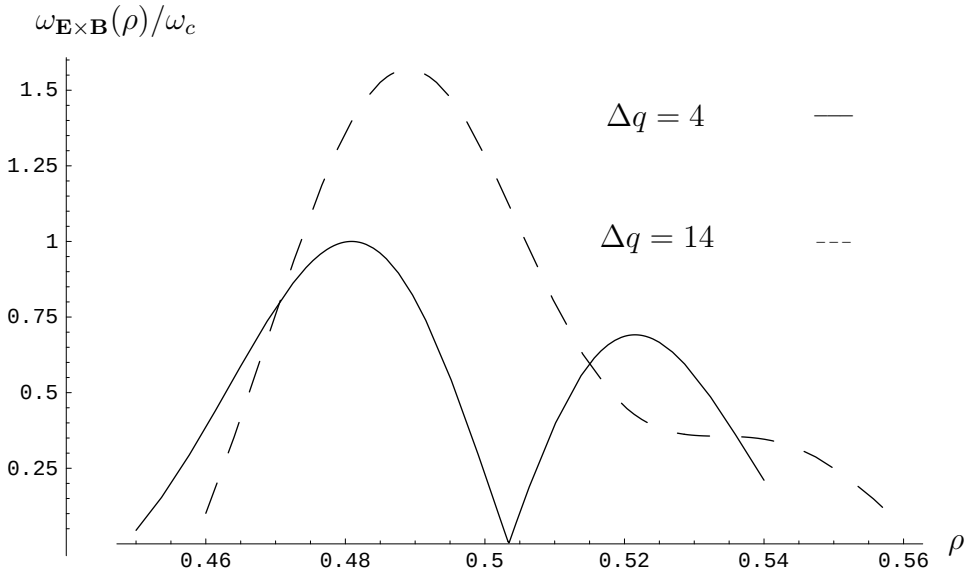

Figure 17: Increase of the $\omega_{\mathbf{E}\times\mathbf{B}}$ extremum in the $s < 0$ and decrease in the $s > 0$ regions due to the increase of Δq. The profiles are obtained for v_{iz} Gaussian-like and $v_{i\theta} = 0$ and are normalized with respect to the $s < 0$ extremum of $\omega_{\mathbf{E}\times\mathbf{B}}$ for $\Delta q = 4$.

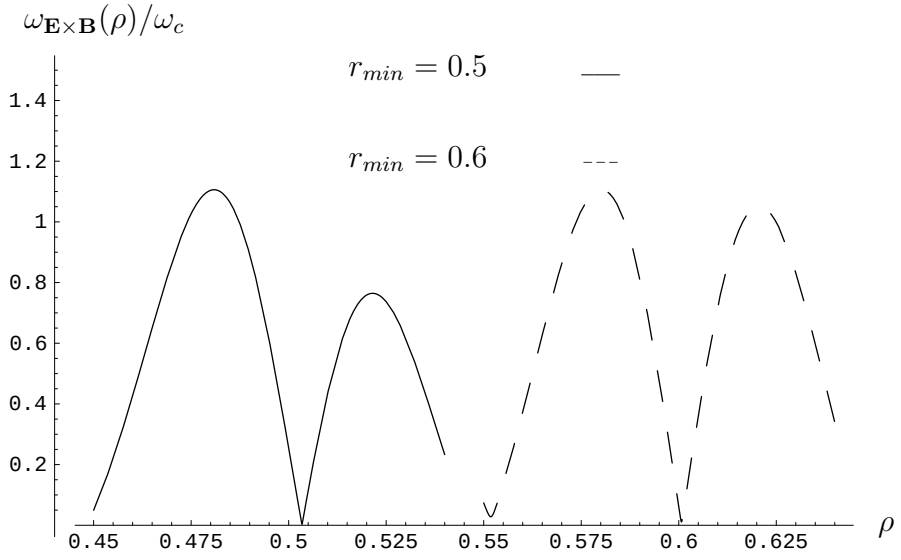

Figure 18: Increase of the normalized $\omega_{\mathbf{E}\times\mathbf{B}}$ maxima due to the outward shift of the position of q_{min} for purely toroidal Gaussian-like flow.

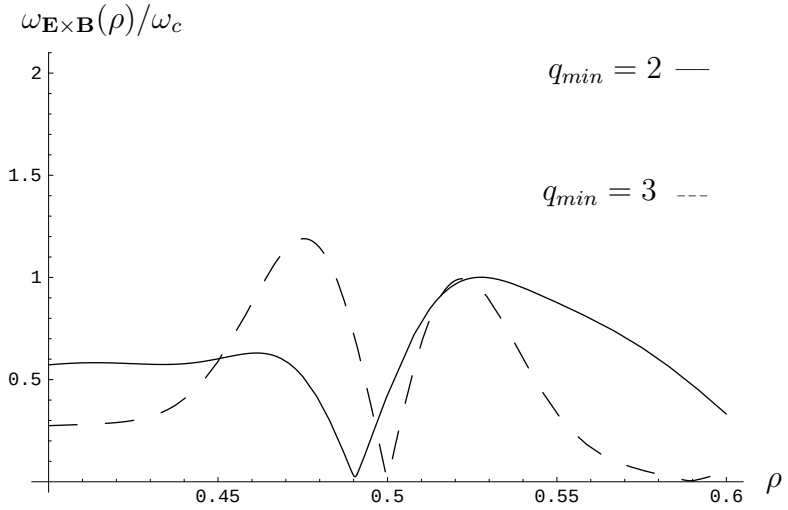

Figure 19: Increase of the $\omega_{\mathbf{E}\times\mathbf{B}}$-extrema as q_{min} takes larger values when both velocity components have Gaussian-like profiles. In this particular case the increase of the extremum in the $s > 0$ region is very small. The profiles are normalized with respect to the $s > 0$ maximum of $\omega_{\mathbf{E}\times\mathbf{B}}$ for $q_{min} = 3$.

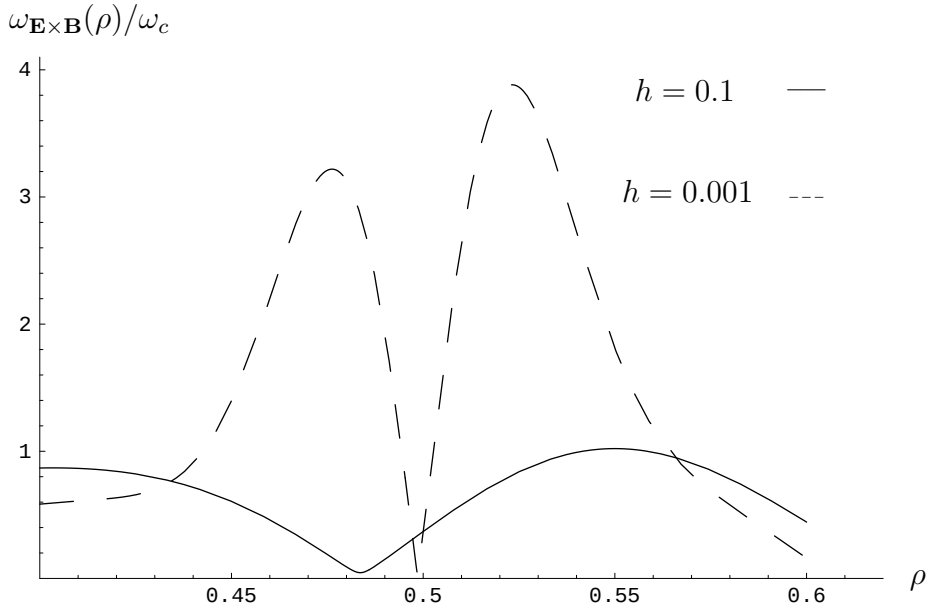

Figure 20: Increase of the $\omega_{\mathbf{E}\times\mathbf{B}}$ extrema caused by the increase of the flow shear for v_{iz} peaked and $v_{i\theta} \neq 0$. The normalization is made with respect to the $\omega_{\mathbf{E}\times\mathbf{B}}$ extremum in the $s > 0$ region for $h = 0.1$.

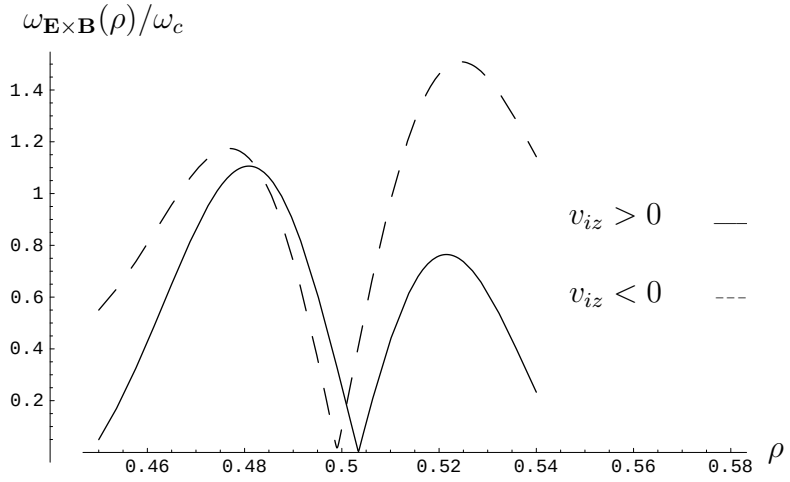

Figure 21: Increase of the normalized $\omega_{\mathbf{E}\times\mathbf{B}}$-extrema caused by inversion of a Gaussian-like toroidal velocity.